Quantum-confined strain gradient effect in semiconductor nanomembranes

R. Binder, B. Gu, and N. H. Kwong
College of Optical Sciences and Department of Physics, University of Arizona, Tucson, Arizona 85721, USA
(Received 19 May 2014; revised manuscript received 23 October 2014; published 26 November 2014)

Semiconductor nanomembranes can exhibit strain gradients that lead to quantum confinement effects similar to the well known quantum-confined Stark effect (QCSE) in semiconductor quantum wells. The deformation of square well into triangular well potential leads to modifications of the exciton resonance, but important differences between the quantum-confined strain gradient effect (QCsgE) and the QCSE include (i) the versatility of the QCsgE in which conduction and valence bands can have different slopes (even reverse slopes are possible), and (ii) the fact that in the QCsgE exciton shifts are determined by the gradients in the heavy-hole and light-hole energies as well as a gradient in the heavy-hole and light-hole coupling.

DOI: 10.1103/PhysRevB.90.195208 PACS number(s): 78.67.De, 78.20.H−, 78.20.Jq, 78.40.Fy

I. INTRODUCTION

Flexible inorganic crystals, including GaAs nanomembranes, have shown great potential for electronic and optical properties [1–11]. They can be, for example, thin layers attached to elastic plastic substrates [2,4] or free-hanging films [6]. They can also be semiconductor quantum wells that are rolled up in microtubes [1,5,7]. Nanomembranes and nanocantilevers are being used as optomechanical oscillators [8,9,11]. Strain can be used to provide confinement potentials via strain gradients [12,13], and is being utilized to control and trap excitons [14–16] and to control quantum dot emission [17].

In semiconductor optics, one of the most important effects is the quantum-confined Stark effect (QCSE), in which a square well ("particle-in-the-box") potential of a semiconductor quantum well is changed into a triangular potential through the application of a voltage gradient (electric field). The electric field can be an externally applied field, or a field created internally by the material through the piezoelectric effect (i.e., the electric field is created by strains) or spontaneous polarization of the material. The importance of the QCSE is rooted in two aspect. First, the simplicity of the triangular quantum well, with analytical solutions available, makes it attractive for textbook discussions of basic quantum confinement effects (e.g., Refs. [18–20]). Second, the QCSE has become the basis of widespread device applications, such as the electroabsorption modulator (e.g., Ref. [21]). Here the triangular deformation leads to a redshift of the lowest interband optical transition (exciton), along with a reduction of the excitonic absorption strength, because the electrons and holes are pushed into opposite corners of their respective triangular quantum wells, Fig. 1.

The modification of square well potentials into triangular potentials can also be achieved by strain fields in nanomembranes with small cylindrical deformations where the strain is proportional to the radial coordinate. If, for example, the membrane is attached to a cylinder on its left, and the left side of the nanomembrane is neither stretched nor shortened (i.e., it is the so-called neutral plane), then the nanomembrane experiences tensile strain (in the geometry of Fig. 2 the tensile strain is in the vertical direction). The strain is (approximately) proportional to z because the stretched arc lengths are proportional to z [22]. In this sense, the strain can be viewed as being analogous to the electric potential in the QCSE. One could therefore expect that there is a simple one-to-one relation between the electric field (i.e., the voltage gradient) and the strain gradient, as was pointed out in Ref. [23]. But we show in the following that, due to the anisotropic nature of cylindrical deformations, in the QCsgE modifications of the exciton resonance are in general caused by both the strain gradient and the overall (average) level of strain in the nanomembrane. In the QCSE, the overall level of the electric potential is automatically removed from observations of the exciton absorption resonance, which involves *differences* between conduction and valence band energies, because the applied voltage shifts the conduction and valence bands by the same amount. The strain gradient in the QCsgE, however, affects the conduction and valence bands differently. Therefore, exciton shifts contain contributions from the overall (or average) strain across the nanomembrane and the actual strain gradient. The fact that the strain affects the conduction and valence bands differently has additional consequences, which make the strain gradient more versatile than the voltage gradient. In the conventional QCSE, the slopes of the conduction and valence bands are the same. In the case of strain gradients, the slopes are in general different. Also, unlike an applied voltage, the cylindrical strain makes the system anisotropic (in Fig. 2, the vertical x direction experiences either tensile or compressive strain, while the direction perpendicular to the plane of the plot remains strain free). Formally, this anisotropy is related to heavy-hole (hh) light-hole (lh) coupling, which has been studied for the case of *planar* anisotropic deformations of quantum wells in Refs. [24–26] (note that the more conventional application of strain, for example in strained-layer superlattices and strained-layer lasers, does not involve optical anisotropy). In contrast to the QCSE, optical anisotropy is an integral part of the QCsgE. Also, because of the hh-lh coupling the effective hh and lh strain potentials are in general not strictly linear in z even if the strain is. Below we show that the slopes of the conduction and valence bands offer a variety of possibilities. They can be almost parallel, as in the case of an electric field, but their relative direction can also be reversed, as schematically shown in Fig. 1(c). This means that, unlike the electric field case, an exciton resonance can be redshifted

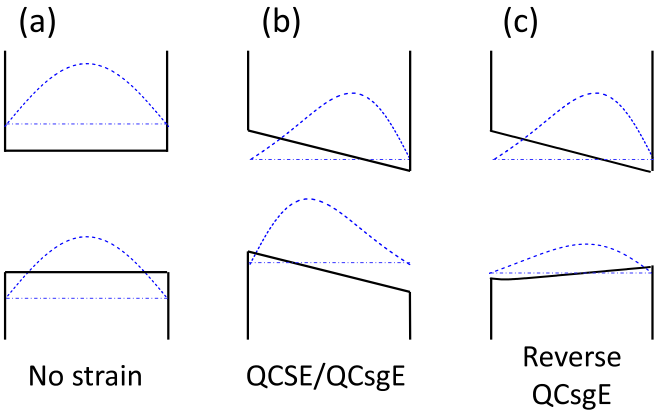

FIG. 1. (Color online) Sketch of square well and triangular well quantum confinement potential of electrons and holes used in the quantum-confined Stark effect QCSE (a) and (b) and found in the quantum-confined strain gradient effect QCsgE (b) as well as the reverse QCsgE (c). Note that the QCsgE does not involve any electric field (for example piezoelectric fields). Also note that in the Stark effect caused by an applied voltage of the form $V_0 + zV'$, the slopes of the conduction (c) and valence (v) bands are equal (they are proportional to V'), and that an overall energy shift of c and v band, which is proportional to V_0 and equal for c and v, does not affect interband transitions and exciton resonances. In the case of strain, both the slopes and the overall energetic shift of the c and v bands are in general different, and the v band is not strictly linear in z. In case of different c- and v-band shifts, we define the QCsgE, in analogy to the QCSE, as the effect solely due to the triangular deformation.

without being reduced in strength. We call this the reverse QCsgE.

II. RESULTS AND DISCUSSION

A. General theory

In order to analyze the QCSgE, we evaluate a fully microscopic theory through numerical integration, which allows us to obtain the (spinor-valued) single-particle wave functions, the energy band structure, and the excitonic absorption spectra of a GaAs nanomembrane. We also discuss simple analytical models that allow us to interpret key features of the full numerical solutions. The details of the theoretical framework have been presented in Ref. [27], but the numerical evaluation in the present study is more general as it does not involve the averaged-strain approximation (in contrast to [27]). The theory involves a 4×4 Luttinger Hamiltonian for the valence bands of the GaAs material as well as the Pikus-Bir strain Hamiltonian (e.g., Refs. [18,28]). Unlike Ref. [27], the wave vector k_z for the motion in z direction is now replaced by $-i\partial/\partial z$, which generates coupled partial differential equations in z for the valence bands and an ordinary differential equation for the conduction band. We apply zero boundary conditions. The differential equations are solved for the in-plane wave vectors $\mathbf{k} = (k_x, k_y)$ through discretization of the z space. The wave functions of the conduction and valence band states are used to compute the electron-hole Coulomb interaction matrix element and the effective dipole-coupling matrix elements. The generalized Wannier equation for the interband polarization, a first-order differential equation in time, is then solved via time stepping. The transmitted and reflected fields are obtained from a transfer matrix formalism. The detailed equations can be found in Ref. [27], see Eqs. (9), (10), and (16). For completeness we have also amended the Luttinger and Pikus-Bir Hamiltonians by the k-linear terms [29,30], using a value of $C_D = 20.6$ meV for the Dresselhaus constant. Hence the difference of the solutions presented in the following and those presented in Ref. [27] are (i) we now discretize the z space in addition to the $\mathbf{k}$ space and thus obtain the proper band structure and z-dependent wave functions, and (ii) the k-linear terms are included.

As for the strain profile of the cylindrically deformed nanomembrane, we utilize a simple analytical model based on the Landau Lifshitz bent plate model, p. 38 of Ref. [31]. That model asserts that, in a thin plate deformed as in Fig. 2, the stresses σ_{xz}, σ_{yz}, and σ_{zz} are essentially zero. We have confirmed, through direct numerical integration of a structural analysis code (Eq. (37) of Ref. [27]), that this is indeed true in our systems (a GaAs quantum well membrane of width 20 nm, with strains of up to approximately 1%). We are using a generalization of the bent plate model to the case of crystals with zincblende symmetry and arbitrary locations of the neutral plane. In particular, we are interested in three different positions of the neutral plane. (i) If the nanomembrane is

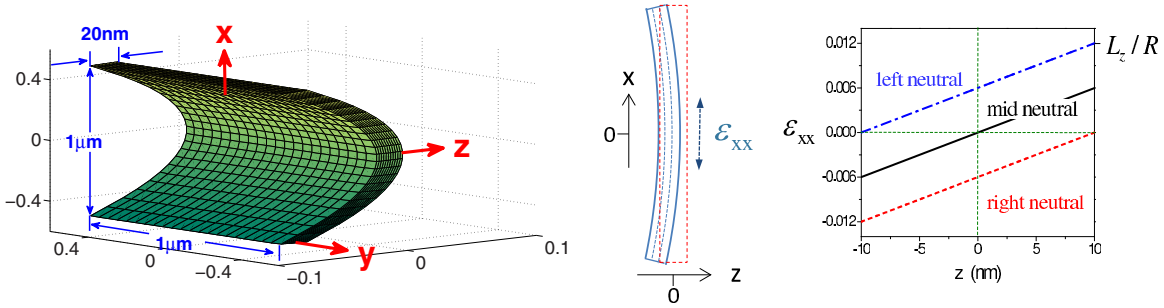

FIG. 2. (Color online) Left: Cylindrical deformation of a nanomembrane. Middle: Sketch viewed from the side. We assume throughout this paper that the nanomembrane is bent to the left. If the arc length of the left (right) side of the bent membrane is the same as the height of the undeformed rectangular membrane shown with red dashed lines, we refer to the deformation as "left neutral" ("right neutral"). If the arc length at the center of the bent membrane is the same as the height of the undeformed rectangular membrane we call this the "mid neutral" deformation. Right: Strain $\epsilon_{xx}(x = 0, z)$ for a nanomembrane of width $L_z = 20$ nm, with an average strain $\bar{\epsilon}_{xx} = \pm 0.6\%$ in the case of left and right neutral deformation. R denotes the cylinder radius.

attached, without strain, to a cylinder on its left (according to Fig. 2), the concave side of the membrane is neutral (we will call this left neutral). (ii) If the membrane is attached to the inside of a cylinder on its right, then the convex side of the membrane is neutral (we will call this right neutral). (iii) It may also be possible, although in practice possibly more difficult, to position the neutral plane in the middle of the membrane, as in the original Landau Lifshitz bent plate model; we will call this mid neutral. For the left (upper sign) and right (lower sign) neutral case, the strain profile, up to linear order in z is given by

$$\epsilon_{xx}(x,z) = [1 \pm L_z/(2R)]\cos(x/R) - 1 + (z/R)\cos(x/R). \quad (1)$$

In order to identify the pure QCsgE, we will focus on the optical response of the nanomembrane's center $|x| \ll R$, so that the cosine function can be equated to unity. Taking absorption spectra over a wider region around the center would lead to inhomogeneous broadening and a dilution of the pure QCsgE. At the center ($x = 0$), the strain reduces to

$$\epsilon_{xx}(z) \equiv \epsilon_{xx}(0,z) = \epsilon^0_{xx} + \epsilon'_{xx} z/L_z, \quad (2)$$

with $\epsilon^0_{xx} = \pm L_z/(2R)$, in the left and right neutral cases. In the mid neutral case, $\epsilon^0_{xx} = 0$. In all three cases, $\epsilon'_{xx} = L_z/R$. In our case, $\epsilon^0_{xx} = 0.1\%$ corresponds to a radius of $R = 10\ \mu$m and is slightly below the fracture threshold [23,32]. The linear strain profiles used below are shown in Fig. 2. Each case corresponds to a different averaged strain, $\bar{\epsilon}_{xx} = (1/L_z)\int dz \epsilon_{xx}(z)$. The strain in z direction follows from the condition that the normal stress in z direction is negligible, $\sigma_{zz} = 0$ and is given by $\epsilon_{zz}(z) \equiv \epsilon_{zz}(0,z) = (-C_{12}/C_{11})\epsilon_{xx}(z)$, where the C_{ij} are the elastic stiffness constants. The corresponding quantum confinement potential for the conduction band states is given by

$$V^c_{st}(z) = E_G + a_c[\epsilon_{xx}(z) + \epsilon_{zz}(z)] + V^c_{\rm conf}(z), \quad (3)$$

where E_G is the bulk band gap and $V^c_{\rm conf}(z)$ is the square well confinement potential. Since the valence band states are governed by the Luttinger and Pikus-Bir Hamiltonians, and since the strain enters both the diagonal and off-diagonal elements of this Hamiltonian, a simple yet rigorous plot of the quantum confinement potential is not possible. However, it is still instructive to look at the diagonal elements of the valence band Hamiltonian at $\mathbf{k} = 0$. In Fig. 3 we show the diagonal confinement potential

$$V^{\rm hh}_{\rm st}(z) = -a_v[\epsilon_{xx}(z) + \epsilon_{zz}(z)] + (b/2)[\epsilon_{xx}(z) - 2\epsilon_{zz}(z)] + V^{\rm hh}_{\rm conf}(z) \quad (4)$$

and

$$V^{\rm lh}_{\rm st}(z) = -a_v[\epsilon_{xx}(z) + \epsilon_{zz}(z)] - (b/2)[\epsilon_{xx}(z) - 2\epsilon_{zz}(z)] + V^{\rm lh}_{\rm conf}(z), \quad (5)$$

which suggest that we should expect an effect similar to the conventional Stark effect in the case of the hh exciton in the right neutral system, while in the left neutral system we should expect the reverse QCsgE with the lowest exciton resonance being dominantly light hole.

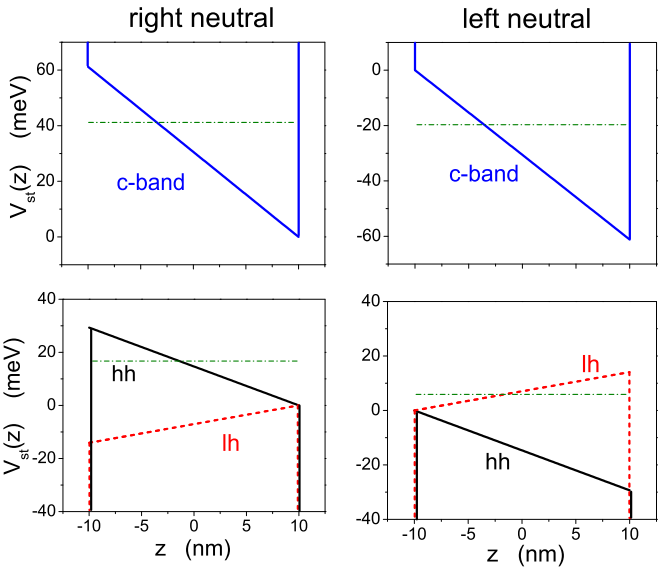

FIG. 3. (Color online) Confinement potential for conduction band electrons (top), and the confinement potential contribution from the diagonal of the Luttinger Hamiltonian for valence band holes. The strain profiles are given in Fig. 2. As in Ref. [27], we use $a_c = -9.3$ eV, $a_v = 1.16$ eV, and $b = -1.9$ eV for the deformation potentials, and $C_{11} = 11.9 \times 10^{11}$ dyn/cm^2, $C_{12} = 5.38 \times 10^{11}$ dyn/cm^2. Dash-dotted lines: Airy solution energies (in left-neutral case calculated with hh mass and lh slope).

B. Exciton spectra

In order to verify our expectations, we show in Fig. 4 exciton spectra obtained from the full microscopic calculation. We first note that in Fig. 4(a) we see a behavior of the hh exciton that is very similar to the conventional Stark effect: the resonance shifts to the red (lower photon energies) and weakens. The mid neutral case does not involve any overall shifts of the c and v band, because the average strain $\bar{\epsilon}_{xx} = 0$. Hence, the changes in the exciton resonance are solely due to the triangular deformation of the confinement potential. Since, however, placing the neutral plane exactly in the middle of the nanomembrane may be more difficult to realize than placing it at the right or left surface, we show in Figs. 4(b) and 4(c) spectra for the right and left neutral case. In these cases, however, we have overall shifts because the average strain $\bar{\epsilon}_{xx}$ is not zero. In order to extract the effect of the triangular deformation, we need to compare systems with a triangular potential to one with a square well potential but the same average strain $\bar{\epsilon}_{xx}$. In the right (left) neutral case, the corresponding square well potential is one of a nanomembrane or quantum well that undergoes planar compressive (tensile) deformation.

The effects of anisotropic planar deformations have been studied and observed [24–26]. Planar compressive (tensile) strain leads to a blue (red) shift and an increase of strength of the lowest exciton for X (Y) polarized light. The shifted resonances are not pure hh excitons, as the strain leads to superpositions of hh and lh wave functions in a way that breaks the x-y symmetry. The strain-induced anisotropy can be understood from the valence band strain Hamiltonian in the

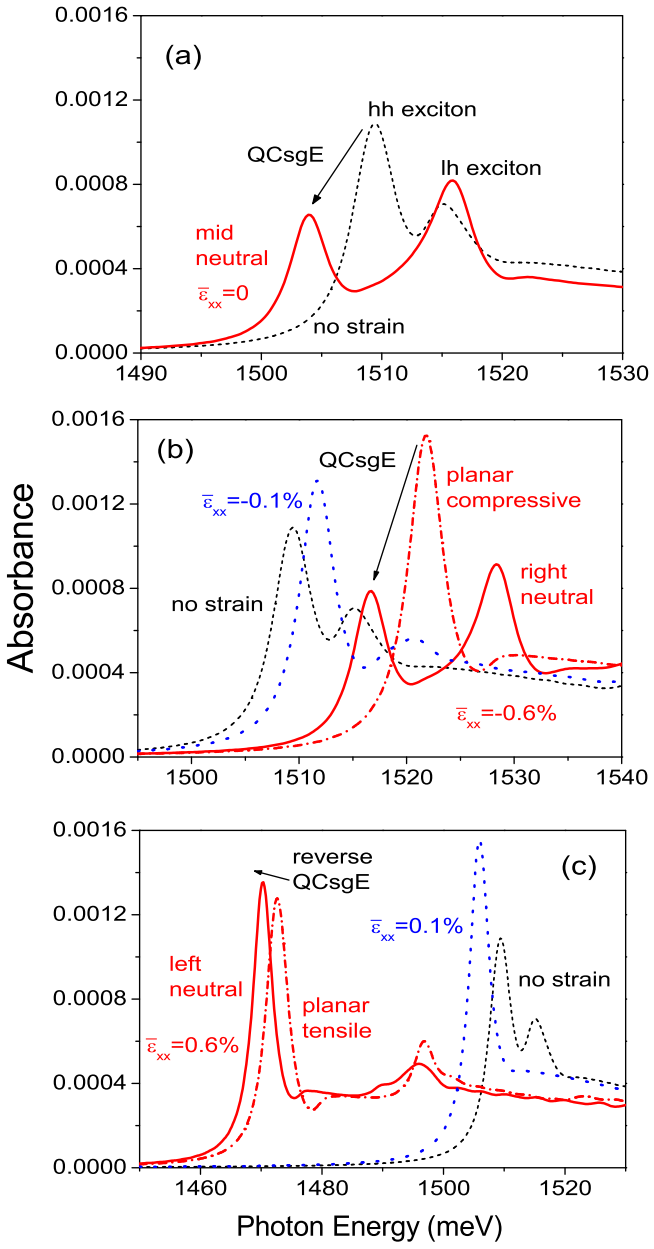

FIG. 4. (Color online) Absorption spectra calculated with the theory outlined in Ref. [27]. The bulk band gap is $E_G = 1500$ meV. Short-dashed black line: unstrained nanomembrane; red solid line: strain with gradient according to Fig. 2; red dash-dotted line: strain without strain gradient (i.e., with square well confinement potential) but same average strain $\bar{\varepsilon}_{xx} = \pm 0.6\%$ as in solid red line; dotted blue line: small strain $\bar{\varepsilon}_{xx} = \pm 0.1\%$ (for this strain value the curves with and without strain gradient are practically the same). Spectra in (a) and (b) for X, in (c) for Y-polarized light.

$(3/2, -1/2)$ subsystem (cf. Eqs. (A5)–(A8) in [27]),

$$\begin{pmatrix} s_+ & c \\ c & s_- - \Delta \end{pmatrix}, \tag{6}$$

with $s_\pm = \bar{\epsilon}_{xx}[-a_v \pm b/2] + \bar{\epsilon}_{zz}[-a_v \mp b]$, $c = -(\sqrt{3}/2)b\bar{\epsilon}_{xx}$, and the hh-lh splitting $\Delta > 0$. To first order in $\bar{\epsilon}_{xx}$ (with $|\bar{\epsilon}_{xx} b| \ll \Delta$), the spin-up components of the eigenvectors are

$$|hh\rangle \sim \left[|x\rangle\left(1 + \frac{b}{2\Delta}\bar{\epsilon}_{xx}\right) + i|y\rangle\left(1 - \frac{b}{2\Delta}\bar{\epsilon}_{xx}\right)\right] \tag{7}$$

and

$$|lh\rangle \sim \left[|x\rangle\left(\frac{3b}{2\Delta}\bar{\epsilon}_{xx} - 1\right) + i|y\rangle\left(\frac{3b}{2\Delta}\bar{\epsilon}_{xx} + 1\right)\right]. \tag{8}$$

For example, since $b < 0$, the hh wave function's $|x\rangle$ ($|y\rangle$) component is increased (decreased) by compressive ($\bar{\epsilon}_{xx} < 0$) strain, thus increasing (decreasing) absorption of X (Y) polarized light.

We see in Fig. 4(b) that, for $\bar{\epsilon}_{xx} = -0.6\%$, the triangular deformation leads to a signature very similar to the conventional Stark effect. The shift can be attributed in large part to the shift of the bands in the triangular deformation, see Fig. 5. The conduction band (not shown) shifts by 2.84 meV down, and the hh valence band at $\mathbf{k} = 0$ by about 3.95 meV up (see Fig. 5). The redshift of the exciton resonance in Fig. 4(b) is about 5.06 meV, which is 1.74 meV less than the shift expected from the band shifts. This difference can be attributed to the fact that the valence band shifts depend on $\mathbf{k}$, and also the fact that the Coulomb interaction is modified due to the change of wave functions entering the Coulomb form factor. The reduction in the exciton strength can be attributed to a reduction of wave function overlap (see next paragraph). In Fig. 4(c) we see that the left neutral case also leads to a redshift. But in contrast to the conventional case, where the redshift is associated with a reduction in the exciton strength, here the exciton does not get reduced by the triangular deformation. The size of the redshift, here about 2.34 meV, is again slightly less than what would be expected on the basis of the conduction and valence band shifts brought about by the triangular deformation (2.85 meV from the c band and 0.59 meV from the v band, see Fig. 5). Figure 5 shows that the Airy solutions using the hh mass and the highest valence band slopes (Fig. 3) yield almost exactly the QCsgE shift in the mid neutral case, indicating a compensation of the strain-induced shift resulting from the compressive strain on the left side of the nanomembrane by hh-lh coupling effects.

The Airy solutions under (over) estimate the shift in the right (left) neutral case. This is expected because in the right (left) neutral case the wave functions are pushed into a corner where the strain is more compressive (tensile) than average, resulting in a strain-induced shift to higher (lower) valence band energies not accounted for by the Airy solution. For the conduction band, the Airy solutions and the numerical solutions are the same.

The reduction in the exciton strength in Fig. 4(b) can be attributed to a reduction of wave function overlap. The valence band wave functions are, in general, four-component spinors for angular momentum labels $j = 3/2, -1/2, 1/2, -3/2$. We show the wave functions corresponding to the lowest exciton resonance in Fig. 6 for $\mathbf{k} = 0$, in which case the $3/2$, $-1/2$ and $1/2$, $-3/2$ subsystems are decoupled and the wave functions have only two spinor components.

The mid neutral case shows that the wave functions are pushed to the left, opposite to the case of c-band electrons, which are pushed to the right. The wave function, while still dominantly of hh character (i.e., the $3/2$ component is large), acquires a small portion of lh character ($-1/2$ component).

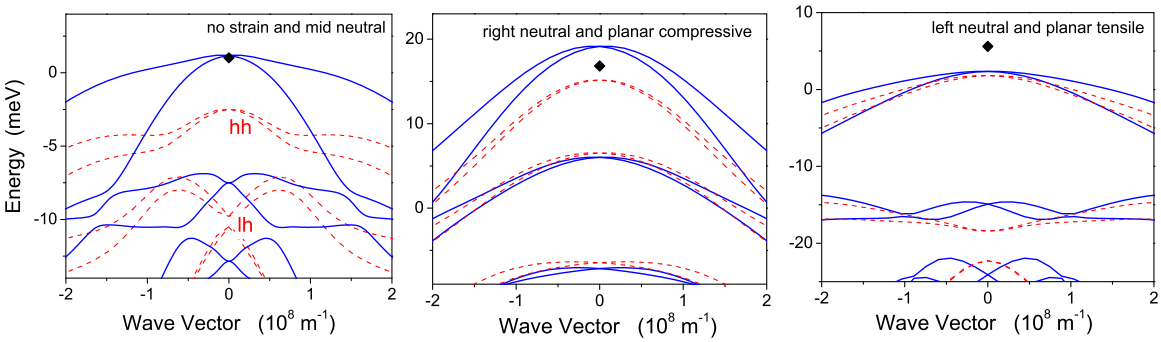

FIG. 5. (Color online) Valence band structure without (red dashed lines) and with (solid blue lines) strain gradients. The strain profiles are given in Fig. 2. The right neutral and planar compressive (left neutral and planar tensile) systems have the same average strain $\bar{\epsilon}_{xx} = -0.6\%$ ($\bar{\epsilon}_{xx} = +0.6\%$). The planar systems do not have strain gradients. Shown are the first six valence bands. The twofold spin degeneracy is lifted by the strain, leaving only Kramer's degeneracy [$E(\mathbf{k}) = E(-\mathbf{k})$]. Without strain, the spin degeneracy is lifted by the k-linear terms in the Luttinger Hamiltonian. The valence band strain-gradient shift for the lowest exciton can be deduced from the difference between the highest red dashed and solid blue bands. Diamonds show Airy solutions for highest valence bands at $\mathbf{k} = 0$ (cf. Fig. 3).

In the left neutral case, the wave function is dominantly of lh character (large $-1/2$ contribution) and is pushed to the right side; both effects in agreement with the simplified argument based on Fig. 3. The lack of reduction of the oscillator strength stems, in part, from the fact that the hole wave function is pushed to the same side as the c-band wave function. The small increase in exciton strength compared to the square well with the same average strain can be ascribed to the fact that, on the right side ($z > 0$), the strain is more tensile than the average. Therefore, looking with y-polarized light, the lowest exciton resonance is expected to grow.

C. Proposal for experimental observation

The strict definition of the QCsgE requires comparison of nanomembranes that differ only in the triangular deformation, not the overall shift of the bands, but it may be difficult in practice to perform such a comparison. A simpler demonstration of the QCsgE could be based on a comparison of cylindrically deformed nanomembranes with increasing deformation. Figure 7 shows the hh and lh exciton peak positions, read off "by hand" from the exciton spectra calculated with the full microscopic theory, with and without triangular deformation. In the planar deformation case (i.e.,

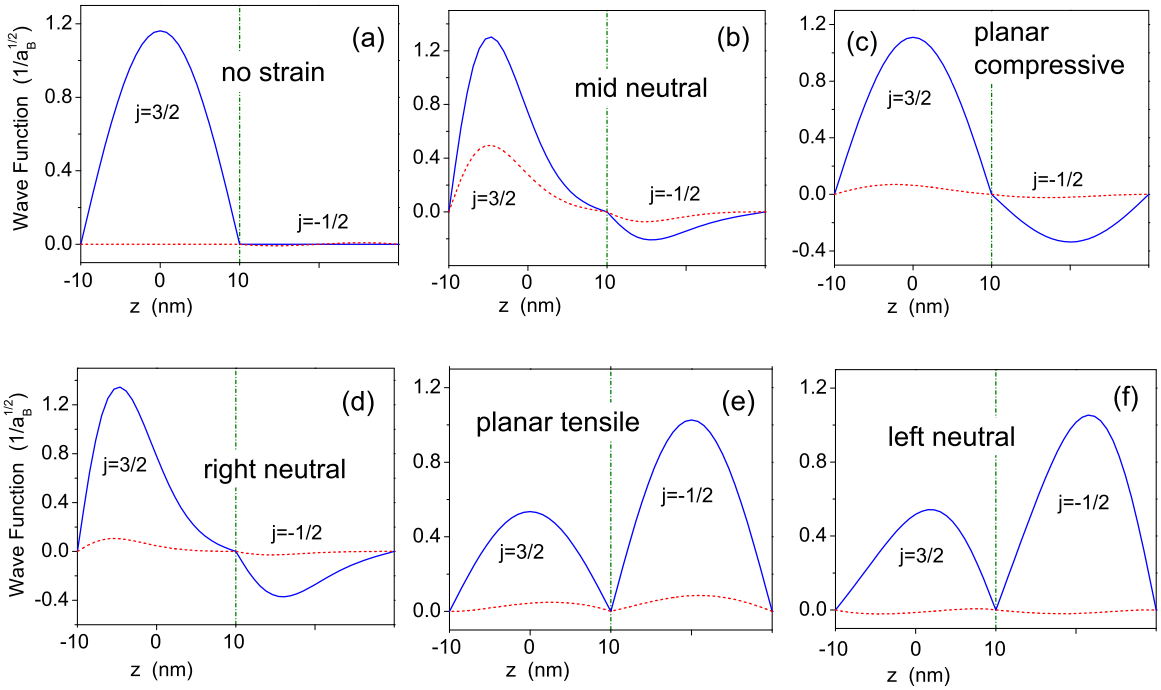

FIG. 6. (Color online) Spinor-valued wave functions at $\mathbf{k} = 0$ of the highest valence band. Blue solid line: real part, red dashed line: imaginary part. For clarity, the light-hole components $j = -1/2$ are shifted horizontally. The corresponding conduction band wave function (not shown) is pushed to the right by the strain gradient. Mid neutral and right neutral show that the hole wave functions are pushed to the left (normal QCsgE), whereas the left neutral wave function is pushed to the right (reverse QCsgE) and becomes predominantly light hole ($j = -1/2$). Bohr radius $a_B = 13.5$ nm.

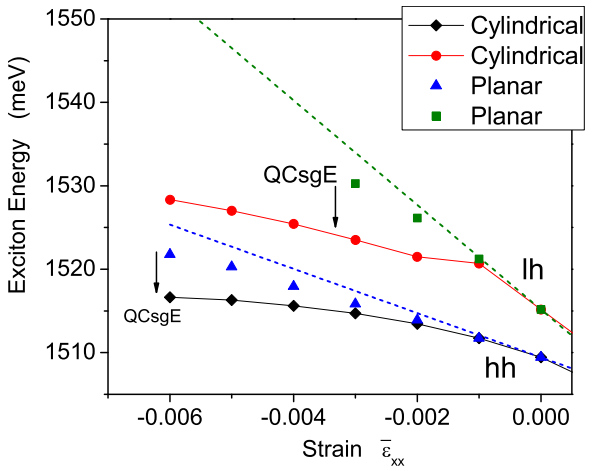

FIG. 7. (Color online) Exciton peak positions for cylindrical deformation (left neutral, $\bar{\epsilon}_{xx} > 0$) and corresponding square well potentials (planar deformation). The lh-exciton peak vanishes for $\bar{\epsilon}_{xx} < -0.003$, hence no green square symbols are shown at those strains. At $\bar{\epsilon}_{xx} \neq 0$, hh (lh) is used as a label without implying dominantly $j = \pm 3/2$ ($\pm 1/2$) wave functions at $\mathbf{k} = 0$. The dashed lines show the analytical model (see text).

without triangular deformation) the exciton peaks agree well with the following simple analytic model. Using the $\mathbf{k} = 0$ conduction and valence band Hamiltonian (Eqs. (10) and (A5)–(A8) in Ref. [27]), we form a 2×2 matrix,

$$\begin{pmatrix} h_+ & -c \\ -c & h_- \end{pmatrix}, \tag{9}$$

with $h_\pm = E^x_{\mathrm{hh/lh}} + \bar{\epsilon}_{xx}[a \mp b/2] + \bar{\epsilon}_{zz}[a \pm b]$, where $a = a_c + a_v$ is the interband hydrostatic deformation potential, and we have replaced the $\mathbf{k} = 0$ transition energies by the hh and lh exciton energies E^x_{hh} and E^x_{lh} for the case without strain. The eigenvalues of this 2×2 matrix can easily be found analytically and are plotted as dashed lines in Fig. 7. The QCsgE can now be identified as a redshift relative to peak positions predicted by this simple model for the planar deformation case. The effect is particularly strong on the compressive side ($\bar{\epsilon}_{xx} < 0$).

D. Conclusion

In summary, we have defined the quantum-confined strain gradient effect as the shift of exciton resonances (together with possible change of their oscillator strengths), brought about by a triangular deformation of an otherwise square well potential. We have taken care to extract effects solely due to the triangular deformation, and not to count shifts and/or changes in the oscillator strength due to z-averaged anisotropic deformation. We found that the QCsgE exhibits similarities, but also distinct differences from the well-known quantum-confined Stark effect. These differences, notably the fact that conduction and valence band triangular confinement potentials are generally not equal, and that they can even be reversed, make the QCsgE an interesting topic for further exploration. Moreover, it will be interesting to investigate a variety of systems used in optomechanics as well as systems in the which electric fields, for example in the form of piezoelectric fields, coexists with the quantum-confined strain gradient effect.

ACKNOWLEDGMENTS

One of us (B.G.) gratefully acknowledges financial support from the Technology and Research Initiative Fund (TRIF), Arizona.

[1] N. Ohtani *et al.*, Physica E **21**, 732 (2004).
[2] Y. Sun, E. Menard, and J. A. Rogers, Appl. Phys. Lett. **88**, 183509 (2006).
[3] L. Zhang, L. Dong, and B. J. Nelson, Appl. Phys. Lett. **92**, 243102 (2008).
[4] H. C. Ko *et al.*, Nature (London) **454**, 748 (2008).
[5] Y. Mei *et al.*, ACS Nano **3**, 1663 (2009).
[6] P. Cendula, S. Kiravittaya, Y. F. Mei, C. Deneke, and O. G. Schmidt, Phys. Rev. B **79**, 085429 (2009).
[7] C. Deneke *et al.*, Appl. Phys. Lett. **96**, 143101 (2010).
[8] M. Hossein-Zadeh and K. J. Vahala, IEEE J. Select. Topics Quantum Electron. **16**, 276 (2010).
[9] K. Usami *et al.*, Nat. Phys. **8**, 168 (2012).
[10] J. Snyder *et al.*, Proc. Natl. Acad. Sci. USA **110**, 18425 (2013).
[11] A. Salmon, M. Capener, J. Baumberg, and S. Elliott, Measure. Sci. Technol. **25**, 015202 (2014).
[12] K. Kash, B. P. Van der Gaag, D. D. Mahoney, A. S. Gozdz, L. T. Florez, J. P. Harbison, and M. D. Sturge, Phys. Rev. Lett. **67**, 1326 (1991).
[13] Y. Zhang, Phys. Rev. B **49**, 14352 (1994).
[14] D. W. Snoke, V. Negoita, and K. Eberl, J. Lumin. **87-89**, 157 (2000).
[15] N. Naka, J. Omachi, and M. Kuwata-Gonokami, Phys. Rev. B **76**, 193202 (2007).
[16] N. W. Sinclair, J. K. Wuenschell, Z. Vörös, B. Nelsen, D. W. Snoke, M. H. Szymanska, A. Chin, J. Keeling, L. N. Pfeiffer, and K. W. West, Phys. Rev. B **83**, 245304 (2011).
[17] G. J. Beirne, M. Reischle, R. Roßbach, W.-M. Schulz, M. Jetter, J. Seebeck, P. Gartner, C. Gies, F. Jahnke, and P. Michler, Phys. Rev. B **75**, 195302 (2007).
[18] S. Chuang, *Physics of Optoelectronic Devices* (Wiley-Interscience, New York, 1995).
[19] H. Haug and S. W. Koch, *Quantum Theory of the Optical and Electronic Properties of Semiconductors*, 4th ed. (World Scientific, Singapore, 2004).
[20] D. Miller, *Quantum Mechanics for Scientist and Engineers* (Cambridge University Press, Cambridge, 2008).
[21] N. Frateschi *et al.*, Electron. Lett. **40**, 140 (2004).
[22] K. Kubota *et al.*, Physica E **13**, 313 (2002).
[23] P. Cendula, S. Kiravittaya, and O. Schmidt, J. Appl. Phys. **111**, 043105 (2012).

[24] H. Shen, M. Wraback, J. Pamulapati, P. G. Newman, M. Dutta, Y. Lu, and H. C. Kuo, Phys. Rev. B **47**, 13933(R) (1993).
[25] M. Wraback, H. Shen, J. Pamulapati, P. G. Newman, and M. Dutta, Phys. Rev. Lett. **74**, 1466 (1995).
[26] M. Wraback *et al.*, Appl. Phys. Lett. **74**, 507 (1999).
[27] B. Gu and R. Binder, J. Opt. Soc. Am. B **29**, A60 (2012).
[28] W. W. Chow and S. W. Koch, *Semiconductor-Laser Fundamentals* (Springer, Berlin, 1999).
[29] E. Kane, Semiconductor Semimetals **1**, 75 (1966).
[30] D. A. Broido and L. J. Sham, Phys. Rev. B **31**, 888 (1985).
[31] L. Landau and E. Lifshitz, *Theory of Elasticity*, 3rd ed. (Pergamon, Oxford, 1986), Chaps. I and II.
[32] Y. Sun *et al.*, Nat. Nanotechnol. **1**, 201 (2006).